VNU Journal of Science: Mathematics - Physics
Journal homepage: https://js.vnu.edu.vn/MaP

Original Article

Comparative Study of Strain and In-plane Electric Field Effects On Valley Polarization in the Magneto-optical Absorption Spectrum of a Borophene Monolayer

Doan Minh Quang[1], Mai Thi Hue[2] Nguyen Thi Thuy[2], Ta Thi Tho[2,*]

[1]*VNU University of Science, 334 Nguyen Trai, Thanh Xuan, Hanoi, Vietnam*
[2]*Hanoi Universityof Civil Engineering, 55 Giai Phong, Bach Mai, Hanoi, Vietnam*

Received 26th April 2025
Revised 15th August 2025; Accepted 30th September 2025

Abstract: Borophene allotropes possess a variety of captivating physical properties, making them promising for numerous applications in practical devices. In this study, we theoretically explore the magneto-optical absorption of an $8-Pmmn$ borophene monolayer subjected to an optical field and a perpendicular static magnetic field considering the combined effect of an in-plane electric field and mechanical strain. The magneto-optical absorption coefficient is calculated using perturbation theory, assuming a degenerate electron gas at low temperatures. The results indicate that valley polarization in the optical absorption coefficient can only be achieved when the in-plane electric field and/or strain is applied to the system. The valley polarization varies gradually with the electric field and becomes significant only at high electric field strengths. On the other hand, the valley polarization is highly sensitive to strain. For the K (K') valley, the absorption spectrum shows a red (blue) shift, with the intensity of the absorption peaks increasing (decreasing) as the strain becomes stronger. Additionally, the valley polarization strongly depends on the external magnetic field and the incident photon energy. For the given values of electric field and strain, as the external magnetic field increases, the polarization weakens. The above observations suggest that the combined effects of the factors on the valley polarization need to be considered systematically. The present results are significant for the application of strain and electric field engineering in valleytronics and flexible optoelectronic devices.

Keywords: Borophene; Tilted Dirac cones; Magneto-optical absorption; Valley polarization; Strain; Electric field.

* Corresponding author.
E-mail address: thott@huce.edu.vn

https//doi.org/10.25073/2588-1124/vnumap.5017

1. Introduction

In conventional electronics, electrical charge is employed for data encoding. However, the movement of this charge leads to heat generation, which restricts the size and integration density of circuits, thus limiting the switching (on and off) speed. Conversely, the spin and valley degrees of freedom are fundamental attributes of electrons, playing a crucial role in the development of next-generation electronics. Spintronics utilizes the spin states of electrons as quantum bits to store information, enabling quicker switching speeds, reduced energy use, and the miniaturization of devices [1-5]. This has led to considerable interest in spintronics using semiconductors and metals over recent decades. In a similar vein, valleytronics takes advantage of the valley degree of freedom in electrons for data encoding and processing [6-14]. Valleys represent local minima found at various points in a material's energy band structure within the Brillouin zone. This innovative approach, distinct from traditional electronics, offers potential for creating energy-efficient devices with enhanced functionalities and improved data storage capabilities through the manipulation of electron density and dynamics in these valleys. Valleytronic technologies could be pivotal for the future of semiconductor advancements, integrating developments in both spintronics and optoelectronics.

Typically, materials with tilted and anisotropic energy dispersion cones exhibit pronounced valley polarization in their physical properties, making them suitable materials for valleytronics applications, particularly two-dimensional (2D) materials [6, 15-21]. Among 2D borophene structures, $8-Pmmn$ borophene shows substantial promise for applications in valleytronics [22-28]. Research findings indicate that $8-Pmmn$ borophene features an energy spectrum characterized by tilted and anisotropic Dirac cones. Importantly, when subjected to external electromagnetic fields or strain, these Dirac cones demonstrate significant valley polarization, which can influence other electronic transport characteristics [26, 29-34]. In Ref. [29], the authors studied the effect of tilted Dirac cones in $8-Pmmn$ borophene on its magnetotransport properties when subjected to periodic modulations. The magnetoconductivity was calculated using linear response theory in the low-temperature regime. The application of weak spatial modulations, such as an electric field, a magnetic field, or both, induces a nonzero oscillatory drift velocity that is dependent of the magnetic field, leading to Weiss oscillations in the longitudinal conductivity at weak magnetic field. Notably, the results show that the presence of both out-of-phase electric and magnetic modulations can cause significant valley polarization in the longitudinal conductivity. The valley polarization is shown to arise from the opposite tilting of the two Dirac cones at the K and K' valleys. S. K. F. Islam studied the impact of strain on the longitudinal and Hall conductivities in $8-Pmmn$ borophene [26]. The results reveal that when the strained borophene sheet is exposed to an in-plane electric field (Hall field), the valley dependence is primarily governed by the strain rather than the Hall field. Additionally, if the real (external) magnetic field is substituted by the pseudo-magnetic field induced by strain, the electric field loses its ability to induce valley-polarized transport. In a recent work [35], Tho et al. have calculated the optical absorption coefficient of the $8-Pmmn$ borophene monolayer when subjected to a perpendicular magnetic field in the presence of an in-plane electric field. The results indicate that the tilt of the Dirac cones leads to a redshift of the absorption peaks. The simultaneous presence of an in-plane electric field and the tilt parameter breaks the valley degeneracy in the Landau levels, resulting in valley polarization in the optical absorption coefficient, that does not occur without the in-plane electric field and/or the tilt parameter.

In this study, we investigate simultaneous effects of mechanical strain and an external electric field on the valley polarization in the magneto-optical absorption spectrum of monolayer borophene $8-Pmmn$. The impact of mechanical strain, in addition to the electric field, is expected to lead to interesting features in the absorption spectrum. The optical absorption coefficient of an electromagnetic wave by electrons in the system is calculated using perturbation theory when the system is placed in a

static, uniform magnetic field while subjected to an external in-plane electric field and strain. To clearly illustrate the competitive effects of the electric field and strain, numerical calculations of valley polarization are conducted and analyzed in detail. The paper is structured as follows. In Sec. II, we present the theoretical model and expression for the optical absorption coefficient. Sec. III presents numerical results. We end the paper with a summary of the work in Sec. IV.

2. Theoretical Framework

2.1. Electronic States in $8-Pmmn$ *Borophene Monolayer*

In this investigation, we consider a monolayer of $8-Pmmn$ borophene placed within the $x-y$ plane of the Cartesian coordinate system. The low-energy effective Hamiltonian for Dirac fermions in the system is given by [25-27, 29]

$$\mathcal{H} = \xi\left(v_x p_x \sigma_x + v_y p_y \sigma_y + v_t p_y \mathbb{I}\right) \tag{1}$$

where $\xi = \pm 1$ corresponds to the valley K (for $\xi = +1$) and K' (for $\xi = -1$), with the velocities $\{v_x, v_y, v_z\} = \{0.86, 0.69, 0.32\}$ expressed in units of $v_0 = 10^6$ m/s. Here, $\sigma = (\sigma_x, \sigma_y)$ are the pseudo-Pauli matrices, and $\mathbb{I}$ denotes the identity matrix. $\vec{p} = (p_x, p_y)$ is the momentum of carriers in 2D plane. It is important to note that, in contrast to the isotropic Dirac cones of graphene, the velocities along the $x-$ and $y-$directions in $8-Pmmn$ borophene are not equal. The presence of a non-zero v_t term in the Hamiltonian reflects the inherent tilt of the Dirac cones in the energy dispersion. The Hamiltonian above can be diagonalized to yield the energy dispersion relation as [25-27,29]

$$E_{\xi,\lambda,\vec{k}} = \xi \hbar v_t k_y + \lambda \hbar \sqrt{v_x^2 k_x^2 + v_y^2 k_y^2}. \tag{2}$$

Here, $\lambda = \pm 1$ indicates the band index, and $\vec{k} = (k_x, k_y)$ represents the carrier 2D wave vector. The inclusion of the v_t term causes the Dirac cones to tilt along the k_y-direction. However, the tilting of the two Dirac cones at the two valleys occurs in opposite directions. It is worth noting that this tilting disrupts the particle-hole symmetry in the $8-Pmmn$ borophene structure. Additionally, the tilt impacts the group velocity, especially along the $y-$direction, potentially affecting electronic properties like the Fermi velocity and the carrier dynamics within the material.

The monolayer is now exposed simultaneously to a uniform static magnetic field, an electric field, and a strain. The magnetic field is oriented perpendicular to the plane of the monolayer, given by $\vec{B} = (0, 0, B)$, while the in-plane electric field is specified as $\vec{E}_r = (E_r, 0, 0)$. Additionally, we model the strain as generating a pseudo-magnetic field, with the strain-induced vector potentials in the two valleys having opposite signs [25]. Similar strain-induced pseudo-magnetic effects have been reported in graphene [36-38] and Weyl semimetals [39,40]. The Hamiltonian for the $8-Pmmn$ borophene monolayer, incorporating the effects of the magnetic field, electric field, and strain, is expressed as [26]

$$\mathcal{H} = \xi\left[v_x p_x \sigma_x + v_y (p_y + eA_S)\sigma_y + v_t (p_y + eA_S)\mathbb{I}\right] + eE_r x\mathbb{I}, \tag{3}$$

in which $A_S = x(B + \xi t)$ represents the vector potential resulting from real magnetic field (B) and strain, where t (in the same units with B) is the pseudo-magnetic field induced by the strain and e is

the absolute value of electron charge. The eigenfunctions and eigenvalues corresponding to the Hamiltonian (3) are given, respectively, as [26]

$$E_\zeta = \lambda \mathrm{h}\omega_\xi \sqrt{2n}\left(1-\beta_\xi^2\right)^{3/4} - \mathrm{h}k_y\left(\frac{E_r}{B+\xi t}\right), \tag{4}$$

$$\Psi_\zeta(\mathrm{r}\vec{r}) \equiv |\zeta\rangle = \frac{\mathrm{e}^{\mathrm{i}k_y y}}{\sqrt{2L_y\gamma_\xi}}\left[\begin{pmatrix}\cosh(\theta_\xi/2)\\ -\mathrm{i}\sinh(\theta_\xi/2)\end{pmatrix}\lambda\phi_n(X') - \mathrm{i}\xi\begin{pmatrix}-\mathrm{i}\sinh(\theta_\xi/2)\\ \cosh(\theta_\xi/2)\end{pmatrix}\phi_{n-1}(X')\right], \tag{5}$$

where $\zeta = \{n, \xi, \lambda, k_y\}$, $n = 1,2,3,\ldots$ denotes the Landau levels (LLs), L_y is the normalization length along the $y-$direction, $\vec{r} = (x,y)$ is the 2D position vector of carrier, $\beta_\xi = [E_r/(B+\xi t) + \xi v_t]/\sqrt{v_x v_y}$, $\gamma_\xi = 1/\sqrt{1-\beta_\xi^2}$, $\omega_\xi = v_c/l_\xi$ is the cyclotron frequency with $v_c = \sqrt{v_x v_y}$ and $l_\xi = \sqrt{\mathrm{h}/e(B+\xi t)}$ being the magnetic length, $\phi_n(X')$ are the wave function of harmonic oscillators, $X' = \frac{(1-\beta_\xi^2)^{1/4}}{l_\xi}\left[x + k_y l_\xi^2 + \lambda\sqrt{2n}l_\xi\beta_\xi/(1-\beta_\xi^2)^{1/4}\right]$, and the angle θ_ξ is determined by $\tanh\theta_\xi = \beta_\xi$. The $n=0$ state (the ground state) is treated separately and the corresponding eigenfunction is given by

$$\Psi_{\{0,\xi,\lambda,k_y\}}(\mathrm{r}\vec{r}) = \frac{\mathrm{e}^{\mathrm{i}k_y y}}{\sqrt{2L_y\gamma_\xi}}\left[\lambda\begin{pmatrix}\cosh(\theta_\xi/2)\\ -\mathrm{i}\sinh(\theta_\xi/2)\end{pmatrix}\phi_0(X')\right]. \tag{6}$$

It is evident that the effects of the electric field and strain on the electronic states are expressed quite complexly through characteristic quantities such as the cyclotron frequency ω_ξ, the magnetic length l_ξ, and the tilt parameter β_ξ, which is associated with the valley index ξ. This contrasts with the strain- and electric field-free case, where these quantities are independent of the valley index [26].

2.2. Analytical result for the magneto-optical absorption coefficient

Based on the above eigenfunctions and eigenvalues, we now calculate the optical absorption coefficient in the $8-Pmmn$ borophene monolayer when an EMW of frequency ω and the polarization vector being in the $y-$direction. Within the assumption of a degenerate electron gas at low temperatures in this calculation, the optical absorption coefficient for the absorption of photon is given by [41-43]

$$\Gamma^{(\xi)} = \frac{2\pi\sqrt{\epsilon_r}}{c\mathrm{h}N_f}\sum_{\zeta,\zeta'} f(E_\zeta)\left[1-f(E_{\zeta'})\right]|\langle\zeta'|H_R|\zeta\rangle|^2\,\delta(E_\zeta - E_{\zeta'} + \mathrm{h}\omega), \tag{7}$$

where c is the speed of light in vacuum, N_f is the photon number, ϵ_r is the dielectric constant or relative permittivity of the material [26], $f(E_\zeta)$ is the Fermi distribution function of carriers, the delta function $\delta(x)$ ensures the law of conservation of energy of the processes, $\langle\zeta'|H_R|\zeta\rangle$ is the matrix element of electron-photon interaction corresponding to the following Hamiltonian [41-43]

$$H_R = -\frac{\mathrm{i}e\mathrm{h}}{m_\mathrm{e}}\sqrt{\frac{2\pi\mathrm{h}N_f}{\epsilon_0\epsilon_r\omega V_0}}\frac{\partial}{\partial x}, \tag{8}$$

for the case of the polarization vector being in the $x-$ direction. Here, $\epsilon_0 = 8.86\times10^{-12}$ $\mathrm{C^2N^{-1}m^{-2}}$ is the electric constant, V_0 is the sample volume, and m_e is the carrier effective mass, developed previously in Refs. [44-45] and sometimes referred to as the optical effective mass [46], which is applicable for an arbitrary energy dispersion including non-parabolic energy dispersion materials such as graphene or $8-Pmmn$ borophene with linear energy dispersion. From Eqs. (5) and (6), the matrix elements for H_R in (8) can be obtained and then substituted into Eq. (7) of the absorption coefficient. After a straightforward calculation with the help of transformation $\sum_{k_y} \to \frac{L_y}{2\pi}\int_0^{L_x/l_\xi^2} dk_y$, one has

$$
\begin{aligned}
\Gamma^{(\xi)} = {} & \frac{\Gamma^0}{2}\sum_{\lambda,\lambda'} f_{E_{0,\xi,\lambda}}(1-f_{E_{1,\xi,\lambda'}})\delta(E_{0,\xi,\lambda}-E_{1,\xi,\lambda'}+\mathrm{h}\omega) \\
& + \Gamma^0\sum_{\lambda,\lambda'}\sum_{n\geq1}\Big[\Big(n+\frac{1}{2}\Big) f_{E_{n,\xi,\lambda}}(1-f_{E_{n+1,\xi,\lambda'}})\delta(E_{n,\xi,\lambda}-E_{n+1,\xi,\lambda'}+\mathrm{h}\omega) \\
& + \Big(n-\frac{1}{2}\Big) f_{E_{n,\xi,\lambda}}(1-f_{E_{n-1,\xi,\lambda'}})\delta(E_{n,\xi,\lambda}-E_{n-1,\xi,\lambda'}+\mathrm{h}\omega)\Big] \\
& + \beta_\xi^2\Gamma^0\sum_{\lambda,\lambda'}\sum_{n\geq1}\Big[\frac{(n-1)}{2} f_{E_{n,\xi,\lambda}}(1-f_{E_{n-2,\xi,\lambda'}})\delta(E_{n,\xi,\lambda}-E_{n-2,\xi,\lambda'}+\mathrm{h}\omega) \\
& + \frac{(n+1)}{2} f_{E_{n,\xi,\lambda}}(1-f_{E_{n+2,\xi,\lambda'}})\delta(E_{n,\xi,\lambda}-E_{n+2,\xi,\lambda'}+\mathrm{h}\omega)\Big]
\end{aligned}
\tag{9}
$$

where $\Gamma^0 = \pi e^2\mathrm{h}^2(1-\beta_\xi^2)^{1/2}/(2cm_\mathrm{e}^2\epsilon_0\sqrt{\epsilon_r}\omega l_\xi^4 d)$, $E_{n,\xi,\lambda} = \lambda\mathrm{h}\omega_\xi\sqrt{2n}\big(1-\beta_\xi^2\big)^{3/4}$, and d is the vertical thickness of the layer. It should be mentioned that, unlike the result obtained in [35], here the quantities appearing in the absorption coefficient, such as the magnetic length (l_ξ), tilt parameter (β_ξ), and electron energy ($E_{n,\xi,\lambda}$), depend on both the electric field and the strain. Therefore, the dependence of the optical absorption coefficient on the electric field and strain is expected to reveal interesting properties, which will be further clarified in the next section (Sec. III).

3. Numerical Results

This section is dedicated to the numerical evaluation of the MOAC derived earlier, aiming to demonstrate the behavior of the absorption spectrum. To prevent the divergence of the delta functions in Eq. (9), we adopt the following replacement:

$$
\delta(E_{n,\xi,\lambda}-E_{n',\xi',\lambda'}+\mathrm{h}\omega) = \frac{\pi^{-1}\gamma_0}{\gamma_0^2+(E_{n,\xi,\lambda}-E_{n',\xi',\lambda'}+\mathrm{h}\omega)^2},
\tag{10}
$$

where γ_0 is a phenomenological broadening parameter, chosen here as $\gamma_0 = 0.05\mathrm{h}\omega_c$ [26]. In the following calculations, we focus on the undoped system, setting the Fermi level to zero. Therefore, only interband optical transitions of electrons are considered, which corresponds to choosing $\lambda=-1$ and $\lambda'=+1$. Also, $d = 2.18\text{Å}$ and $\epsilon_r = 10$ are taken [26].

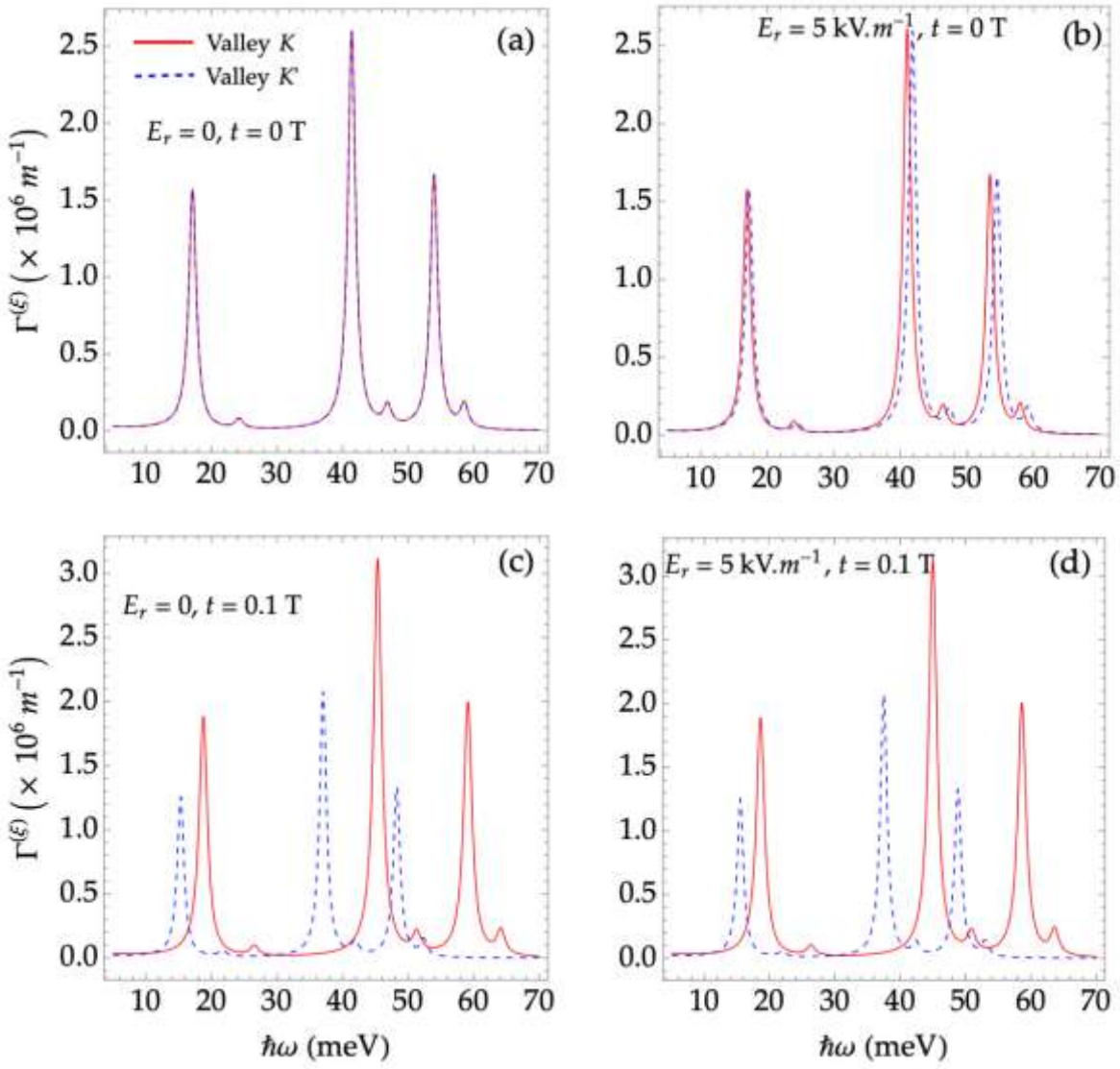

Figure 1. Magneto-optical absorption spectrum for different scenarios of electric field and strain: (a) absence of both electric field and strain; (b) with an electric field of 5 kV.m^{-1} and no strain; (c) with a strain of 0.1 T and no electric field; and (d) with both electric field and strain. In all cases, the real magnetic field is $B = 0.5$ T, the temperature is $T = 4.2$ K, and the LLs $n = 0 \div 2$ are considered.

In Fig. 1, we plot the absorption spectra in the K valley ($\xi = +1$, solid red lines) and K' valley ($\xi = -1$, dashed blue lines) as functions of photon energy, at a fixed magnetic field of $B = 0.5$ T, for different scenarios involving electric field and strain. It can be observed that the absorption spectra display series of principal peaks, along with lower supplement peaks. The principal peaks arise from electronic transitions between adjacent Landau levels ($n \to n \pm 1$), while the supplement peaks result from transitions between Landau levels separated by one level ($n \to n \pm 2$) due to the absorption of

photon. These are typical cyclotron resonance peaks, which are commonly observed in the magneto-optical absorption spectra of materials subjected to a strong magnetic field. Additionally, from left to right, the first principal peak is resulted from the transitions $E_{1,\xi,-1} \rightarrow E_{0,\xi,+1}$ and $E_{0,\xi,-1} \rightarrow E_{1,\xi,+1}$; the second principal peak corresponds to the transitions $E_{1,\xi,-1} \rightarrow E_{2,\xi,+1}$ and $E_{2,\xi,-1} \rightarrow E_{1,\xi,+1}$; and the third principal peak corresponds to the transitions $E_{3,\xi,-1} \rightarrow E_{2,\xi,+1}$ and $E_{2,\xi,-1} \rightarrow E_{3,\xi,+1}$. We have this because we are considering interband optical transitions, so the photon energy at resonance is then: $\hbar\omega_{res} = E_{n',\xi,+1} - E_{n,\xi,-1} = \sqrt{2}\left(\sqrt{n'} + \sqrt{n}\right)\hbar\omega_\xi\left(1 - \beta_\xi^2\right)^{3/4}$. Therefore, it is clear that the resonance peaks at the highest photon energy values correspond to electron transitions between two Landau levels with the highest indices (differing by one), where one level is in the valence band ($\lambda = -1$) and the other is in the conduction band ($\lambda = +1$), and vice versa. Figure 1(a) illustrates the case where neither in-plane electric field nor strain is applied. In this case, the absorption spectrum shows no valley splitting. In Figs. 1(b), 1(c), and 1(d), we consider the following situations, respectively: the presence of an electric field $E_r = 5\,\text{kV.m}^{-1}$ without strain; the presence of strain with $t = 0.1T$ without the electric field; and the simultaneous presence of both strain and electric field with the values specified above. It can be seen that the presence of an electric field and/or strain induces a noticeable difference in the magneto-optical absorption spectra between the two valleys. This is the condition required for valley polarization in the absorption spectrum, which can be achieved by applying an electric field, strain, or both. In addition, from Figs. 1(a-d), an interesting behavior can be observed: the most pronounced differences in the absorption spectra between the two valleys under the presence of an electric field and/or strain appear at the resonance peaks corresponding to interband transitions between Landau levels with the highest indices (the peaks on the right side of the figures). This will be explained in more detail below, where we plot the Landau levels as a function of the external magnetic field under different conditions of electric field and strain.

To clarify the relationship between the shift of resonant absorption peaks in Fig. 1 and the changes in Landau energy levels, as well as the differences in absorption spectra between the two valleys under varying electric field and strain, in Fig. 2 we plot some first Landau levels as a function of the external magnetic field for the different combinations of electric field and strain considered in Fig. 1. It can be seen that in the absence of both electric field and strain, the Landau levels between the two valleys are completely degenerate (the blue and red curves completely overlap), as shown in Fig. 2(a), resulting in the ovelap of the absorption spectra between the two valleys in Fig. 1(a). However, when the electric field and/or strain is nonzero, this degeneracy is lifted, and valley polarization of the Landau levels emerges. In particular, when strain is present, the Landau levels in the two valleys differ significantly, leading to a pronounced difference in the absorption spectra of the two valleys, as observed in Figs. 1(c) and 1(d). Specifically, if we look closely at a curve corresponding to a Landau level with $n \neq 0$, we will see that the shift in the value of the Landau levels in the presence of strain and/or an electric field is opposite in the two valleys. For example, for convenience, let us consider the values of the Landau levels with $n \neq 0$ at the magnetic field $B = 0.8$ T in Figs. 2(a) ($t = 0$) and 2(c) ($t = 0.1$ T). It can be seen that when strain is present, the Landau energy level of a given state shifts in opposite directions: in the K (K') valley, the Landau energy is higher (lower) compared to it when there is no strain. Mathematically, this behavior is reflected through the frequency ω_ξ and the coefficient β_ξ in Eq. (4), where ω_ξ and β_ξ change in opposite ways in the K valley ($\xi = +1$) and the K' valley ($\xi = -1$) under the influence of strain. The opposite changes in the Landau levels as well as the absorption spectrum in the two valleys under strain can be physically explained by the anisotropic crystal structure of *8*-Pmmn borophene. This leads to the Dirac dispersion cones in the two valleys tilting in opposite directions, resulting in opposite responses of the electrons in these two valleys to the external electric field and/or strain. Additionally, we can also provide a mathematical explanation for why the difference in the absorption spectra between

the two valleys becomes more pronounced at the resonance peaks corresponding to higher photon energies, and vice versa, as follows. From the resonance condition $\hbar\omega_{res} = E_{n',\xi,+1} - E_{n,\xi,-1} = \sqrt{2}\left(\sqrt{n'} + \sqrt{n}\right)\hbar\omega_{\xi}\left(1-\beta_{\xi}^{2}\right)^{3/4}$, considering a resonance peak corresponding to the transition $n \rightarrow n'$, the difference in photon energy between this resonance peak in the valley *K* and the corresponding resonance peak in the valley K′ is: $\Delta = \hbar\omega_{res(\xi=+1)} - \hbar\omega_{res(\xi=-1)} = \sqrt{2}\left(\sqrt{n'} + \sqrt{n}\right)\left[\hbar\omega_{\xi=+1}\left(1-\beta_{\xi=+1}^{2}\right)^{3/4} - \hbar\omega_{\xi=-1}\left(1-\beta_{\xi=-1}^{2}\right)^{3/4}\right]$. As a result, the value of Δ becomes large when *n* and *n'* are large. On the other hand, as we have shown in Figure 1 above, the resonance peaks in the high photon energy region correspond to interband optical transitions between Landau levels with large indices (*n* and *n′* are large), and vice versa. Therefore, the difference in the positions of corresponding absorption peaks between the two valleys is large (small) at high (low) photon energy values.

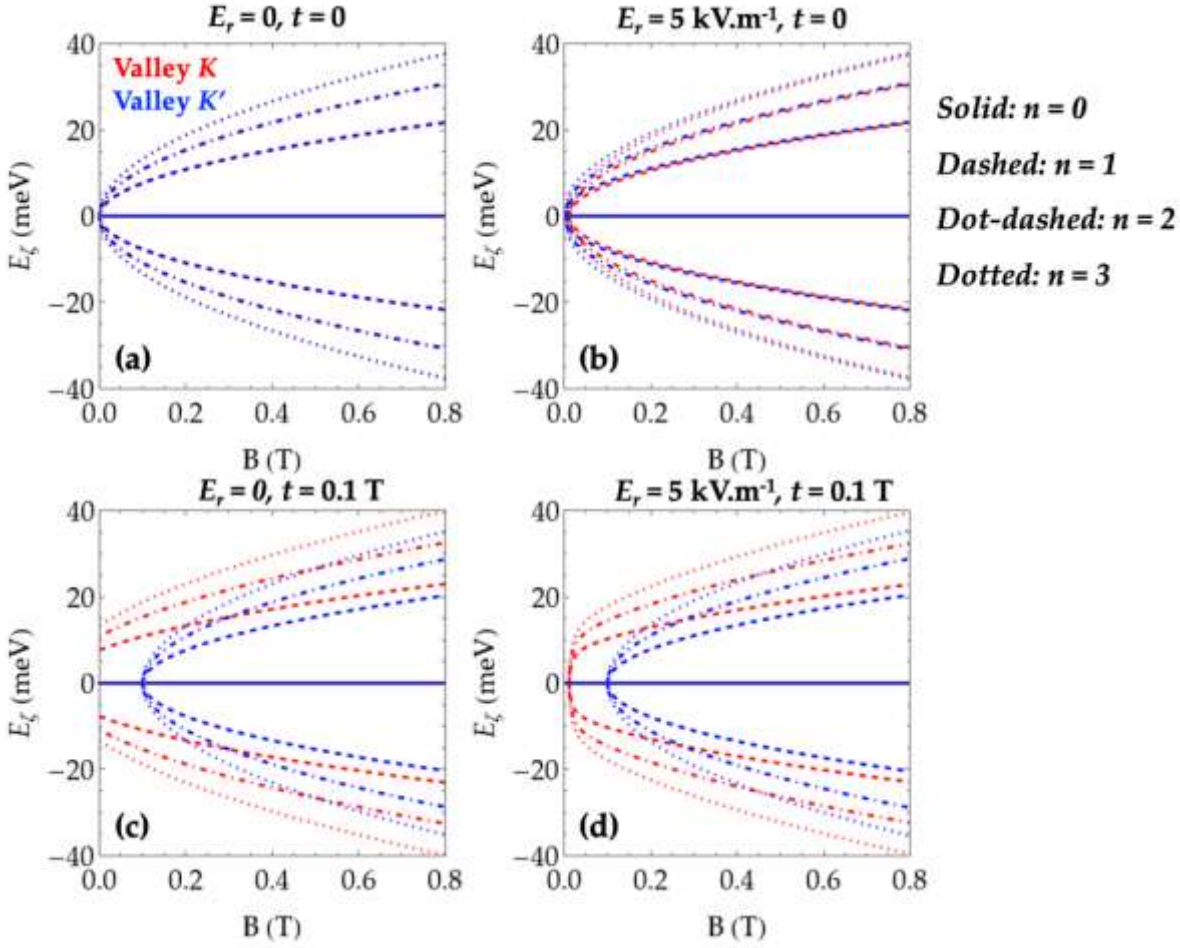

Figure 2. Some of the first Landau energy levels as functions of the external magnetic field for different scenarios of electric field and strain considered in Fig. 1. The red (blue) lines correspond to the *K* (*K*') valley. The solid, dashed, dot-dashed, and dotted lines correspond to the Landau levels *n* = 0, 1, 2, and 3, respectively. The change of the Landau levels with electric field and strain, as well as their differences between the two valleys, explains the difference in absorption spectra between the two valleys in Fig. 1.

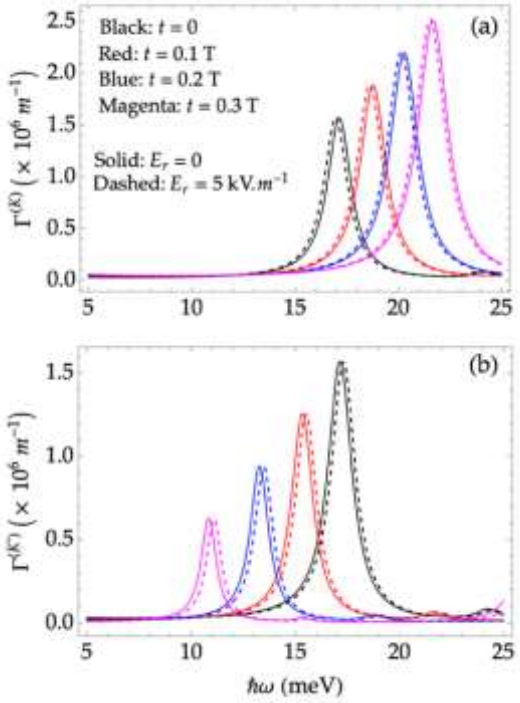

Figure 3. Comparison of absorption spectra between the K ($\xi = +1$) (a) and K' ($\xi = -1$) (b) valleys as the strain t is varied. In all figures, the colors black, red, blue, and magenta represent strains of 0, 0.1, 0.2 and 0.3 T, respectively. The solid and dashed curves correspond to the cases with and without an in-plane electric field, respectively. In all cases, $B = 0.5$ T, $T = 4.2$ K, and $n = 0 \div 2$.

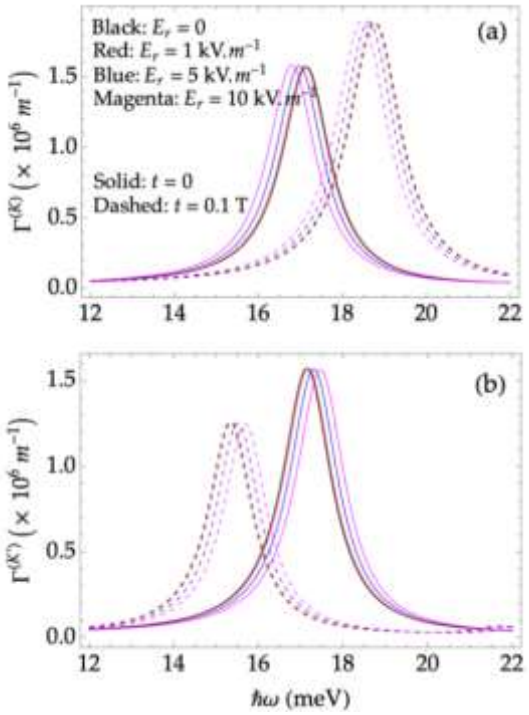

Figure 4. Comparison of absorption spectra between the K ($\xi = +1$) (a) and K' ($\xi = -1$) (b) valleys as the in-plane electric field E_r is varied. In all figures, the colors black, red, blue, and magenta represent electric fields of 0, 1, 2, and 5 kV.m^{-1}, respectively. The solid and dashed curves correspond to the cases with and without strain, respectively. In all cases, $B = 0.5$ T, $T = 4.2$ K, and $n = 0 \div 2$.

To gain a more detailed understanding of how the absorption spectrum changes with electric field and strain, in Fig. 3 we plot the absorption spectra as a function of photon energy for various strain values, both in the absence of an electric field (solid curves) and with an in-plane electric field of $E_r = 5\text{kV.m}^{-1}$ (dashed curves). Figures 3(a) and 3(b) show the results for the K and K' valleys, respectively. From the figure, it is evident that the absorption peaks shift significantly in both position and intensity under the influence of strain. However, only minor changes are observed in the absorption spectrum when the electric field is varied. To illustrate this, we present the absorption spectra for four different values of the electric field, spanning a wide range from zero to ten kilovolts per meter, as depicted in Fig. 4. Once again, we observe that the absorption spectrum remains relatively unchanged despite significant variations in the electric field. From Figs. 3 and 4, we can also observe a very distinct feature: when strain or electric field increases, the absorption spectra in the K and K' valleys show a noticeable difference. Specifically, as strain increases, the absorption peaks in the K (K') valley shift towards higher (lower) photon energy, meaning a blueshift (redshift) occurs, while the height of the

absorption peaks increases (decreases). When the electric field is increased, the absorption peaks in the K valley show a redshift, while the absorption peaks in the K' valley show a blueshift. In short, in the K valley, as the electric field (strain) increases, the absorption spectrum exhibits a redshift (blueshift), and conversely, in the K' valley. Moreover, from Figs. 1(c), 1(d), 3, and 4, it can also be seen that when strain is applied ($t \neq 0$), the intensity of the absorption peaks in the K (K') valley increases (decreases) as the strain increases. This is because, in Eq. (9) for the absorption coefficient, we have $\Gamma^{(\xi)} \sim \Gamma^0 \sim l_\xi^{-4}$, where the magnetic length l_ξ is given by là $l_\xi = \sqrt{\hbar[e(B+\xi t)]^{-1}}$. Clearly, as the strain increases, in the K (K') valley, $l_{\xi=+1}$ ($l_{\xi=-1}$) decreases (increases), leading to the corresponding absorption coefficient increasing (decreasing).

To quantitatively assess the difference in the absorption spectrum between the two valleys, we define the valley polarization in the absorption coefficient as

$$P_v = \frac{\Gamma^{(\xi=+1)} - \Gamma^{(\xi=-1)}}{\Gamma^{(\xi=+1)} + \Gamma^{(\xi=-1)}}. \tag{11}$$

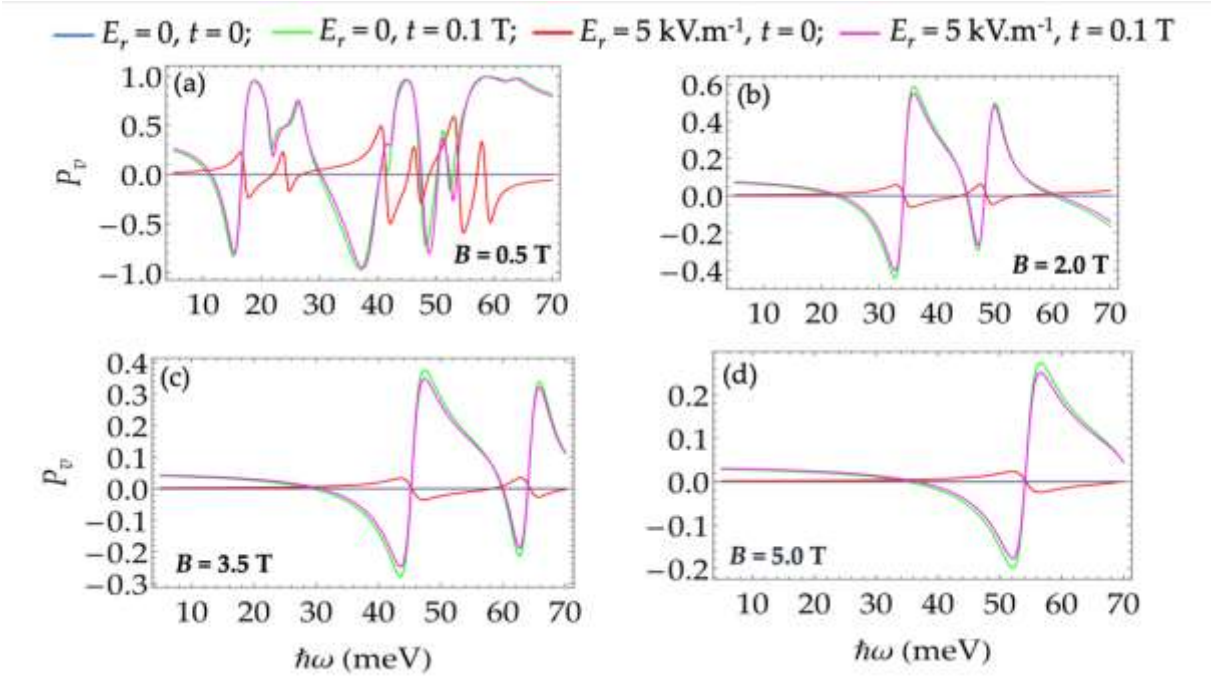

Figure 5. The valley polarization in the absorption coefficient as a function of photon energy for different scenarios of electric field and strain. Figures (a), (b), (c), and (d) correspond to the real external magnetic field of 0.5 T, 2.0 T, 3.5 T, and 5.0 T, respectively. Here, $T = 4.2$ K.

In Fig. 5, we plot the valley polarization as a function of photon energy for different cases of electric field and strain shown in Fig. 1, but at some different values of the real magnetic field. In particular, the parameters in Fig. 5(a) are taken exactly as those in Figs. 1(a)-(d). From Figs. 5(a)-(d), we can see, as expected, that the valley polarization is zero for all photon energy and real magnetic field values when both the electric field and strain are absent (see the blue curves in Figs. 5(a)-(d)), consistent with the result observed in Fig. 5(a). When an electric field ($E_r = 5\,\text{kV.m}^{-1}$) is applied without strain (K'), the

valley polarization appears and oscillates with photon energy. At the real magnetic field of $0.5\mathrm{T}$ presented in Fig. 5(a), the maximum amplitude of valley polarization is approximately 0.59 in the photon energy range of $50-60\,\mathrm{meV}$. When strain is introduced ($t=0.1T$), the valley polarization also appears and oscillates with photon energy, but now the valley polarization at certain photon energy values becomes stronger, both in the presence or absence of the electric field. For example, in Fig. 5(a) for $B=0.5\mathrm{T}$, the valley polarization can reach the value of about 0.99 at photon energy of $60\,\mathrm{meV}$. From Figs. 5(a)-(d), we also observe that, for the selected values of electric field and strain, as the real magnetic field increases, the amplitude of valley polarization decreases. Specifically, when only the strain (electric field) of $0.1\,T$ ($5\ \mathrm{kV.m^{-1}}$) is present, the magnitude of the valley polarization is 0.99 (0.59), 0.59 (0.06), 0.376 (0.035), and 0.273 (0.024) at the real magnetic field of $0.5, 2, 3.5$ and $5\ \mathrm{T}$, respectively. The decrease in valley polarization as the real magnetic field increases can be explained through the dependence of the magnetic length, cyclotron frequency, and tilt parameter on strain, electric field, real magnetic field, and valley index. Recall that $l_\xi=\sqrt{\mathrm{h}[e(B+\xi t)]^{-1}}$, $\omega_\xi=v_c/l_\xi$ and $\beta_\xi=[E_r/(B+\xi t)+\xi v_t]/\sqrt{v_x v_y}$. From this, it can be seen that for fixed values of E_r and t, as B increases the ratio $E_r/(B+\xi t)$ decreases, and the contribution of t to the term $(B+\xi t)$ also becomes less significant, regardless of the value of ξ ($+1$ or -1). This result indicates that, in addition to the individual effect of each factor, the combined influence of these factors on valley polarization is crucial and needs to be systematically considered in their interrelationship.

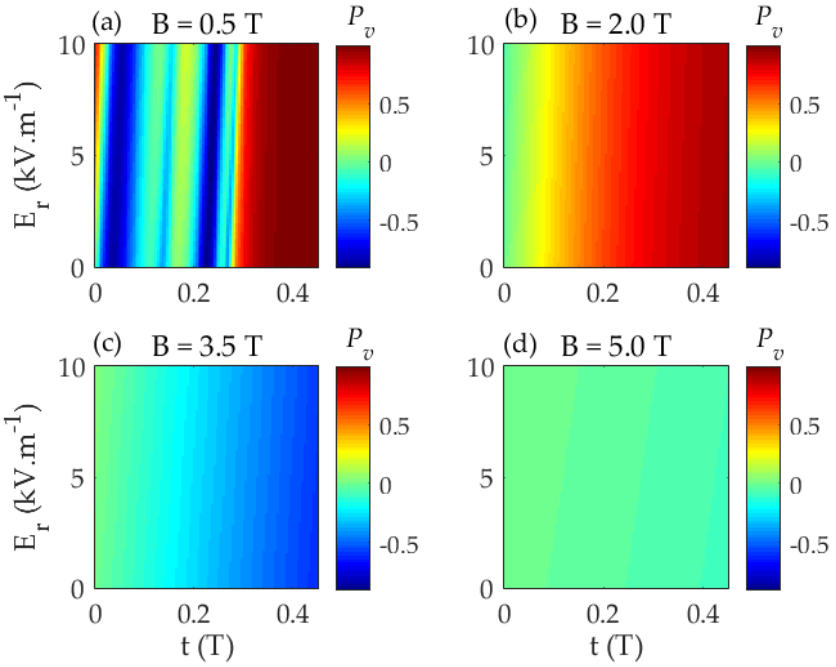

Figure 6. Density plot of the valley polarization versus strain (t) and in-plane electric fied (E_r) at the magnetic field of (a) 0.5 T, (b) 2.0 T, (c) 3.5 T, and (d) 5.0 T. Here, $T=4.2$ K and $\mathrm{h}\omega=40$ meV. Note that all the figures are presented with the same color scale to allow for a comparison of the magnetic field's effect on the valley polarization values.

To gain a broader insight into the competing effects of the electric field and strain on the valley polarization in the magneto-optical absorption spectrum, we present the density plot of valley polarization as a function of the electric field and strain at different values of real magnetic field, shown in Figs. 6(a)-(d). In these plots, we choose $\hbar\omega = 40$ meV because these magnetic field and photon energy values are compatible with each other for interband electronic transitions between several of the lowest Landau levels induced by photon absorption. From Fig. 6, once again we see that the valley polarization is highly sensitive to strain and changes slowly with the electric field (at a fixed strain). At the same time, within the selected range of electric field and strain values, the valley polarization gradually weakens as the real magnetic field increases.

4. Conclusion

We have studied theoretically the effects of an external electric field and strain on valley polarization in the magneto-optical absorption of monolayer borophene $8-Pmmn$ with tilted and anisotropic Dirac cones. The results show that valley polarization in the absorption coefficient can only be achieved when an electric field and/or strain is applied to the system. The valley polarization changes slowly with the electric field and is only significant when the electric field is very strong. In contrast, compared to the electric field, strain induces a much more pronounced change in valley polarization, with the polarization amplitude potentially becoming very large if the strain value is chosen appropriately relative to the external real magnetic field and photon energy. However, for the selected values of electric field and strain, the achieved polarization amplitude also depends on the choice of the real magnetic field and incident photon energy. When the real magnetic field is very strong, the electric field and/or strain must also be increased correspondingly to achieve a significant degree of valley polarization. It can be concluded that, in addition to the independent effects of each factor (electric field, strain, real magnetic field), the combined influence of these factors on valley polarization is crucial and must be considered in their interrelationship in order to achieve the desired polarization, suitable for specific application purposes. The results open up possibility for applications in valleytronics and flexible optoelectronic devices through strain and electric field engineering.

Acknowledgments

This work was completed with the financial support from Hanoi University of Civil Engineering under Grant No. 24-2023/KHXD-TD.

References

[1] I. Žutić, J. Fabian, S. Das Sarma, Spintronics: Fundamentals and applications, Review of Modern Physics, Vol. 76, No. 2, 2004, pp. 323-410, https://doi.org/10.1103/RevModPhys.76.323.

[2] A. Hirohata, K. Yamada, Y. Nakatani, I. L. Prejbeanu, B. Diény, P. Pirro, B. Hillebrands, Review on spintronics: Principles and device applications, Journal of Magnetism and Magnetic Materials, Vol. 509, 2020, pp. 166711, https://doi.org/10.1016/j.jmmm.2020.166711.

[3] V. K. Joshi, Spintronics: A Contemporary Review of Emerging Electronics Devices, Engineering Science and Technology, Vol. 19, No. 3, 2016, pp. 1503-1513, https://doi.org/10.1016/j.jestch.2016.05.002.

[4] G. Yaqin, Z. Xu, H. Zhi, C. Jinyan, L. Zijun, Z. Jing, L. Jingfeng, Z. Zhaowei, Z. Jinkui, H. Xiufeng, W. Hao, Quantum Materials for Spintronic Applications, Npj Spintronics, Vol. 2, No. 1, 2024, pp. 2948-2119, https://doi.org/ 10.1038/s44306-024-00038-z.

[5] R. Priti, J. Bhandari, U. Sheetal, W. Girish, A Review on—Spintronics an Emerging Technology, Silicon, Vol. 14, No. 15, 2022, pp. 9195-9210, https://doi.org/10.1007/s12633-021-01643-x.
[6] S. John, R. Yu, H. Clark, G. Rivera, P. R. Jason, S. Kyle, L. Yao, X. Xiaodong, Transport Signatures of Anisotropic Tilted Dirac Cones in 8-Pmmn Borophene, The European Physical Journal B, Vol. 1, No. 11, 2016, pp. 16055, https://doi.org/10.1038/natrevmats.2016.55.
[7] J. Schaibley, Chapter 10 - Valleytronics in 2D Semiconductors, 2D Materials for Photonic and Optoelectronic Applications, Woodhead Publishing, 2020, pp. 281-302, https://www.sciencedirect.com /B978008102637300003.
[8] X. Rui, Z. Zhiguo, L. Jia, Z. Hanyu, Valleytronics: Fundamental Challenges and Materials Beyond Transition Metal Chalcogenides, Nano micro Small, 2024, pp. 2402139, https://doi.org/10.1002/smll.202402139.
[9] V. A. Steven, N. Daniel, V. O. Joseph, K. Philip, G. Nuh, J. H. Pablo, X. Di, R. Mordechai, Valleytronics: Opportunities, Challenges, and Paths Forward, Small, Vol. 14, No. 38, 2018, pp. 1801483, https://doi.org/10.1002/smll.201801483.
[10] K. Jayakrishna, O. Babita, D. Samal, Valleytronics, Resonance, Vol. 28, No. 4, 2023, pp. 537-546, https://doi.org/10.1007/s12045-023-1581-9.
[11] N. Rohling, G. Burkard, Universal Quantum Computing with Spin and Valley States, New Journal of Physics, Vol. 14, No. 8, 2012, pp. 083008, https://dx.doi.org/10.1088/1367-2630/14/8/083008.
[12] E. A. L. Kuemmeth, G. Steele, K. G. Rasmussen, J. Nygård, K. Flensberg, L. P. A. Kouwenhoven, Valley–spin Qubit in A Carbon Nanotube, Nature Nanotechnology, Vol. 8, No. 8, 2013, pp. 565-568, https://doi.org/10.1038/nnano.2013.140.
[13] D. Culcer, A. L. Saraiva, B. Koiller, X. Hu, S. Das Sarma, Valley-based Noise-resistant Quantum Computation Using Si Quantum Dots, Physical Review Letters, Vol. 108, No. 12, 2012, pp. 126804, https://link.aps.org/doi/10.1103/PhysRevLett.108.126804.
[14] Y. S. Ang, S. A. Yang, C. Zhang, Z. Ma, L. K. Ang, Valleytronics in Merging Dirac Cones: All-electric-Controlled Valley Filter, Valve, and Universal Reversible Logic Gate, Physical Review B, Vol. 96, No. 24, 2017, pp. 245410, https://link.aps.org/doi/10.1103/PhysRevB.96.245410.
[15] A. Rycerz, J. Tworzydło, C. W. J. Beenakker, Valley Filter and Valley Valve in Graphene, Nature Physics, Vol. 3, No. 3, 2007, pp. 172-175, https://doi.org/10.1038/nphys547.
[16] M. S. Mrudul, A. J. Galán, M. Ivanov, G. Dixit, Light-induced Valleytronics in Pristine Graphene, Optica, Vol. 8, No. 3, 2021, pp. 422-427, https://opg.optica.org/optica/abstract.cfm?URI=optica-8-3-422.
[17] X. Zhou, J. Zheng, F. Zhai, Anisotropic and Valley-resolved Beam-splitter Based on a Tilted Dirac System, Communications in Theoretical Physics, Vol. 74, No. 22, 2022, pp. 075701, https://dx.doi.org/10.1088/1572-9494/ac6fc2.
[18] A. Wild, E. Mariani, M. E. Portnoi, Optical Valley Separation in Two-Dimensional Semimetals with Tilted Dirac Cones, Scientific Reports, Vol. 13, No. 1, 2023, pp. 19211, https://doi.org/10.1038/s41598-023-45940-4.
[19] S. H. Zhang, D. F. Shao, Z. A. Wang, J. Yang, W. Yang, E. Y. Tsymbal, Tunneling Valley Hall Effect Driven by Tilted Dirac fermions, Physical Review Letters, Vol. 131, No. 24, 2023, pp. 246301, https://link.aps.org/doi/10.1103/PhysRevLett.131.246301.
[20] N. Rana, G. Dixit, All-optical Ultrafast Valley Switching in Two-Dimensional Materials, Physical Review Applied, Vol. 19, No. 3, 2023, pp. 034056, https://link.aps.org/doi/10.1103/PhysRevApplied.19.034056.
[21] F. Ussolotti, H. Kawai, Z. E. Ooi, V. Chellappan, D. Thian, A. L. C. Pang, K. E. J. Goh, Roadmap on Finding Chiral Valleys: Screening 2D Materials for Valleytronics, Nano Futures, Vol. 2, No. 3, 2018, pp. 032001, https://dx.doi.org/10.1088/2399-1984/aac9d7.
[22] X. F. Zhou, X. Dong, A. R. Oganov, Q. Zhu, Y. Tian, H. T. Wang, Semimetallic Two-dimensional Boron Allotrope with Massless Dirac Fermions, Physical Review Letters, Vol. 112, No. 8, 2014, pp. 085502, https://link.aps.org/doi/10.1103/PhysRevLett.112.085502.
[23] A. L. Bezanilla, P. B. Littlewood, Electronic Properties of 8–Pmmn Borophene, Physical Review B, Vol. 93, No. 24, 2016, pp. 241405, https://link.aps.org/doi/10.1103/PhysRevB.93.241405.
[24] J. Carrete, W. Li, D. A. Broido, L. J. Gallego, N. Mingo, Physically Founded Phonon Dispersions of Few-layer Materials and the Case of Borophene, Materials Research Letters, Vol. 4, No. 4, 2016, pp. 204–211, https://doi.org/10.1080/21663831.2016.1174163.
[25] A. D. Zabolotskiy, Y. E. Lozovik, Strain-induced Pseudomagnetic Field in the Dirac Semimetal Borophene, Physical Review B, Vol. 94, No. 16, 2016, pp. 165403, https://link.aps.org/doi/10.1103/PhysRevB.94.165403.
[26] S. K. F. Islam, Magnetotransport Properties of 8–Pmmn Borophene: Effects of Hall Field and Strain, Journal of Physics: Condensed Matter, Vol. 30, No. 27, 2018, pp. 275301, https://dx.doi.org/10.1088/1361-648X/aac8b3.

[27] S. A. Herrera, G. G. Naumis, Kubo Conductivity for Anisotropic Tilted Dirac Semimetals and Its Application t8–Pmmn Borophene: Role of Frequency, Temperature, and Scattering Limits, Physical Review B, Vol. 100, No. 19, 2019, pp. 195420, https://link.aps.org/doi/10.1103/PhysRevB.100.195420.
[28] B. D. Napitu, Charge and Heat Transport of Doped 8–Pmmn Borophene with and Without Relaxation Time Approximation, Physical Review B, Vol. 107, No. 15, 2023, pp. 155435, https://link.aps.org/doi/10.1103/PhysRevB.107.155435.
[29] S. K. F. Islam, A. M. Jayannavar, Signature of Tilted Dirac Cones in Weiss Oscillations of 8–Pmmn Borophene, Physical Review B, Vol. 96, No. 23, 2017, pp. 235405, https://link.aps.org/doi/10.1103/PhysRevB.96.235405.
[30] B. D. Napitu, Photoinduced Hall Effect and Transport Properties of Irradiated 8–Pmmn Borophene Monolayer, Journal of Applied Physics, Vol. 127, No. 3, 2020, pp. 034303, https://doi.org/10.1063/1.5130025.
[31] T. Cheng, H. Lang, Z. Li, Z. Liu, L. Zhirong, Anisotropic Carrier Mobility in Two-Dimensional Materials with Tilted Dirac Cones: Theory and Application, Physical Chemistry Chemical Physics, Vol. 19, No. 35, 2017, pp. 23942–23950, http://dx.doi.org/10.1039/C7CP03736H.
[32] L. Jing, S. Yanmei, W. Meimei, H. Pan, Novel Electric Field Effects on Magneto-Optical Conductivity in Eight–Pmmn Borophene, Journal of Physics: Condensed Matter, Vol. 33, No. 18, 2021, pp. 185501, https://dx.doi.org/10.1088/1361-648X/abf19e.
[33] V. A. Margulis, E. E. Muryumin, Optical Properties of Two-Dimensional Materials with Tilted Anisotropic Dirac Cones: Theoretical Modeling with Application to Doped 8–Pmmn Borophene, Journal of Optics, Vol. 24, No. 1, 2021, pp. 014002, https://dx.doi.org/10.1088/2040-8986/ac3c31.
[34] N. U. Wahab, Y. Abdullah, Transport Signatures of Anisotropic Tilted Dirac Cones in 8–Pmmn Borophene, The European Physical Journal B, Vol. 95, No. 8, 2022, pp. 123, https://doi.org/10.1140/epjb/s10051-022-00389-8.
[35] T. T. Tho, N. N. Hieu, D. M. Quang, N. Q. Bau, B. D. Hoi, Effects of Tilted Dirac Cones and In-plane Electric Field on the Valley-dependent Magneto-optical Absorption Spectra in Monolayer 8–pmmn Borophene, Physics Letters A, Vol. 457, 2023, pp. 128578, https://doi.org/10.1016/j.physleta.2022.128578.
[36] N. Levy, S. A. Burke, K. L. Meaker, M. Panlasigui, A. Zettl, F. Guinea, A. H. C. Neto, M. F. Crommie, Strain-Induced Pseudo–magnetic Fields Greater Than 300 Tesla in Graphene Nanobubbles, Science, Vol. 329, No. 5991, 2010, pp. 544-547, https://www.science.org/doi/abs/10.1126/science.1191700.
[37] V. M. Pereira, A. H. Castro Neto, Strain engineering of graphene's electronic structure, Physical Review Letters, Vol. 103, No. 4, 2009, pp. 046801, https://link.aps.org/doi/10.1103/PhysRevLett.103.046801.
[38] B. Roy, H. Z. Xiang, K. Yang, Theory of Unconventional Quantum Hall Effect in Strained Graphene, Physical Review B, Vol. 87, No. 12, 2013, pp. 121408, https://link.aps.org/doi/10.1103/PhysRevB.87.121408.
[39] D. I. Pikulin, A. Chen, M. Franz, Chiral Anomaly from Strain-Induced Gauge Fields in Dirac and Weyl Semimetals, Physical Review X, Vol. 6, No. 4, 2016, pp. 041021, https://link.aps.org/doi/10.1103/PhysRevX.6.041021.
[40] S. Yadav, A. Ptok, Landau Levels in Weyl Semimetal Under Uniaxial Strain, Physica B: Condensed Matter, Vol. 698, 2025, pp. 416730, https://doi.org/10.1016/j.physb.2024.416730.
[41] V. A. Margulis, V. V. Karpunin, Resonant Absorption of Electromagnetic Radiation in A Quantum Channel Due to the Scattering of Electrons by Impurities, Optics and Spectroscopy, Vol. 122, No. 7, 2017, pp. 979, https://doi.org/10.1134/S0030400X17060108.
[42] V. A. Margulis, V. V. Karpunin, Resonance Absorption of Electromagnetic Radiation in A Phosphorene Single Layer, Semiconductors, Vol. 53, No. 4, 2019, pp. 458, https://doi.org/ 10.1134/S1063782619040134.
[43] N. G. Galkin, A. V. Shorokhov, V. A. Margulis, Intraband Absorption of Electromagnetic Radiation by Quantum Nanostructures with Parabolic Confinement Potential, Physics of the Solid State, Vol. 43, No. 3, 2001, pp. 530, https://doi.org/10.1134/1.1356134.
[44] W. Zawadzki, S. Klahn, U. Merkt, Semirelativistic Behavior of Electrons in Insb in Crossed Magnetic and Electric Fields, Physical Review Letters, Vol. 55, No. 9, 1985, pp. 983-986, https://link.aps.org/doi/10.1103/PhysRevLett.55.983.
[45] V. Ariel, Effective Mass and Energy-Mass Relationship, arXiv Preprint, arXiv, 1205.3995, 2012, https://arxiv.org/abs/1205.3995 (accessed on: April 1st, 2025).
[46] K. Seeger, Semiconductor Physics: An Introduction, Springer Series in Solid-State Sciences, Springer-Verlag, 9783540114215, 1985, https://books.google.com.vn/books?id=gvl9AAAAIAA (accessed on: April 1st, 2025).